[a]Present address: Department of Physics, University of Utah, Salt Lake City, Utah 84112.

[1]J. N. Koster and U. Müller, to be published.

[2]J. N. Koster, dissertation, University of Karlsruhe, 1980 (unpublished).

[3]J. N. Koster and U. Müller, in *Recent Developments in Theoretical and Experimental Fluid Mechanics*, edited by U. Müller, K. G. Roesner, and B. Schmidt (Springer-Verlag, Berlin, 1979), pp. 367–375, and in *Natural Convection in Enclosures*, edited by K. E. Torrance and I. Catton (American Society of Mechanical Engineers, New York, 1980), HTD-Vol. 3.

[4]D. V. Lyubimov, G. F. Putin, and V. I. Chernatynskii, Dokl. Akad. Nauk SSSR 22, 554 (1977) [Sov. Phys. Dokl. 22, 360 (1977)]; G. F. Putin and E. A. Tkacheva, Fluid Dyn. 14, 1 (1979).

[5]G. Ahlers and R. P. Behringer, Prog. Theor. Phys., Suppl. 64, 186 (1978); J. Maurer and A. Libchaber, J. Phys. (Paris) 40, 419 (1979); J. P. Gollub and S. V. Benson, J. Fluid Mech. 100, 449 (1980); M. Dubois and P. Bergé, J. Phys. (Paris) 42, 167 (1981).

[6]L. N. Howard, in *Proceedings of the Eleventh International Congress on Applied Mechanics, München*, edited by H. Görtler (Springer-Verlag, Berlin, 1964), p. 1109.

[7]B. K. Hartline and C. R. B. Lister, J. Fluid Mech. 79, 379 (1977).

[8]For the derivation of the power law it is assumed that the thickness of the thermal boundary layer is much larger than the gap depth in order to apply the Hele-Shaw cell concept even for the range of the boundary layer. This assumption is valid for moderately high Rayleigh numbers as observations by real-time interferometry have shown.

Particle Exhaust from Plasma Discharges with an Expanded-Boundary Divertor

M. Ali Mahdavi, J. C. DeBoo, C. L. Hsieh, N. Ohyabu, R. D. Stambaugh, and J. C. Wesley

General Atomic Company, San Diego, California 92138

(Received 21 August 1981)

Measurements of the divertor-region plasma characteristics and argon exhaust efficiencies of the expanded-boundary divertor are reported. High plasma and neutral-hydrogen densities ($\sim 10^{14}/\mathrm{cm}^{-3}$) are observed in the divertor region, and the exhaust efficiency for injected argon exceeds 95%. A simple model based on electron heat conduction parallel to the diverted field lines and frictional force due to proton-argon collisions in the divertor region accurately describes the experimental observations.

PACS numbers: 52.25.Kn

The expanded-boundary divertor[1] is a simplified poloidal divertor configuration where the outermost flux surfaces of the plasma are diverted and expanded by coils located outside of the plasma chamber. Bulk plasma properties associated with the expanded-boundary configuration have been reported earlier.[2,3] The magnetic-flux configuration (Fig. 1) and plasma parameters are similar to those reported earlier. The experiments were performed at a plasma current of 380 kA, toroidal field of 20 kG, and line-average plasma density $\bar{n}_e = (1-5)\times 10^{13}$ cm^{-3}. This paper deals with the diverter region plasma characteristics and hydrogen and argon exhaust properties of the configuration. A simple model based on parallel heat conduction in the boundary plasma accurately describes the density of the divertor region plasma and the hydrogen exhaust. Application of the results of the model to the calculation of proton-argon frictional force explains the argon exhaust.

Measurements of the divertor plasma characteristics show marked dependence on the line-

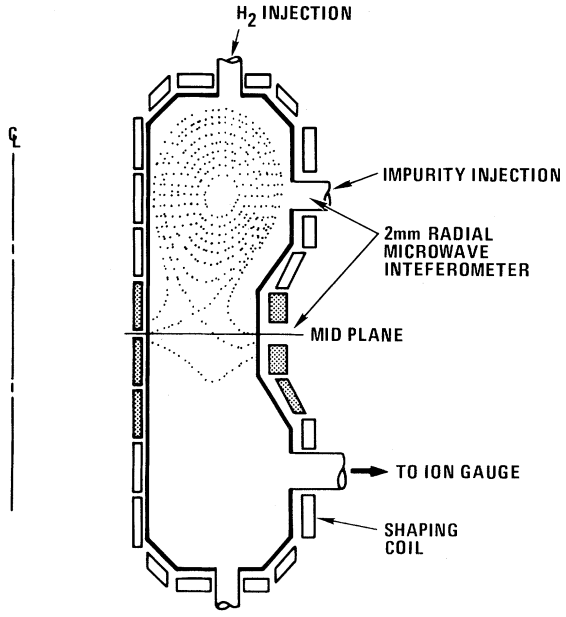

FIG. 1. Cross section of Doublet III with an expanded-boundary flux configuration. The shaping coils used in the formation of the divertor are shaded.

average density of the main discharge. Increasing the main plasma density, $\bar{n}_e$, results in a nonlinear increase in both the divertor line-average density, $\bar{n}_e(l)$, and the neutral pressure, P_G, at the lower ionization gauge [Figs. 2(a) and 2(b)]. At $n_e = 3\times10^{13}$ cm^{-3} the divertor density exceeds the main plasma density, and the neutral pressure reaches $\sim 10^{-3}$ Torr $[n_0(H_2) \sim 3\times10^{13}$ cm$^{-3}]$.

A complete description of the physics of the plasma boundary layer involves particle and energy transport parallel and perpendicular to the flux surfaces, radiation and charge exchange processes, and plasma-wall interactions. However, the density dependence of the boundary plasma can be described by a surprisingly simple model that neglects perpendicular transport, radiation, and particle transport except near the target plate (the wall of the vacuum chamber).

The plasma boundary layer is represented by a plasma channel, of average cross section A, defined by field lines extending from $x = 0$ to $x = l$ (Fig. 3). A power source P_0 exists at $x = 0$ and the lines are terminated by the wall at $x = l$. Particle flow and radiation in the channel are neglected. The electron density at $x = 0$ is assumed to be proportional to $\bar{n}_e$. The boundary is then described by the equations $\nabla_\parallel \cdot \kappa_\parallel \nabla_\parallel k T_e = 0$, and $\nabla_\parallel n_e T_e = 0$, where

$$\kappa_\parallel \equiv \kappa_0 T_e^{5/2}$$

$$= [(4.4\times10^{-12}\text{J/sec deg cm})/Z\ln\boldsymbol{n}]T_e^{5/2}.$$

The boundary conditions are $n_e(0) = \alpha\bar{n}_e$, and $-\kappa_\parallel \nabla_\parallel k T_e = P_0/A$ at $x = 0$, and

$$-\kappa_\parallel \nabla_\parallel k T_e = n_e k T_e (k T_i/2\pi M_i)^{1/2}(\gamma_e + 2T_i/T_e)$$

$$\simeq 8 n_e k T_e (k T_e/2\pi M_i)^{1/2},$$

where α is a proportionality constant and we have used values of the constant γ_e from sheath theory when $T_i > T_e$, but then approximated by setting $T_e = T_i$. Integrating the above equations, we obtain

$$T_e(x)^{7/2} = T_e(0)^{7/2} - 7P_0 x/2\kappa_0 A, \quad (1)$$

where $T_e(0)$ is the solution of

$$T_e(0)^{21/2} = \left(\frac{7P_0 l}{2\kappa_0 A}\right)^7 T_e(0)^7 + \left(\frac{(2\pi M_i)^{1/2} P_0}{\gamma A \alpha \bar{n}}\right)^7, \quad (2)$$

$A = 4\pi R\delta B_p/B_T$, δ is the thickness of the scrape-off layer at $x = 0$, B_T is the toroidal field, B_p is the poloidal field at $x = 0$, and R is the major radius. At sufficiently high densities,

$$\bar{n}_e \gg \frac{(2\pi M_i)^{1/2}}{\alpha\gamma k^{3/2}}\left(\frac{P_0}{A}\right)^{4/7}\left(\frac{2\kappa_0}{7P}\right)^{3/7},$$

$T_e(0)$ assumes a value of $(7lP_0/2\kappa_0 A)^{2/7}$, which is independent of $\bar{n}_e$ and only weakly dependent on parameters such as P_0, l, and δ. In this high-density, conduction-limited heat-flow regime,

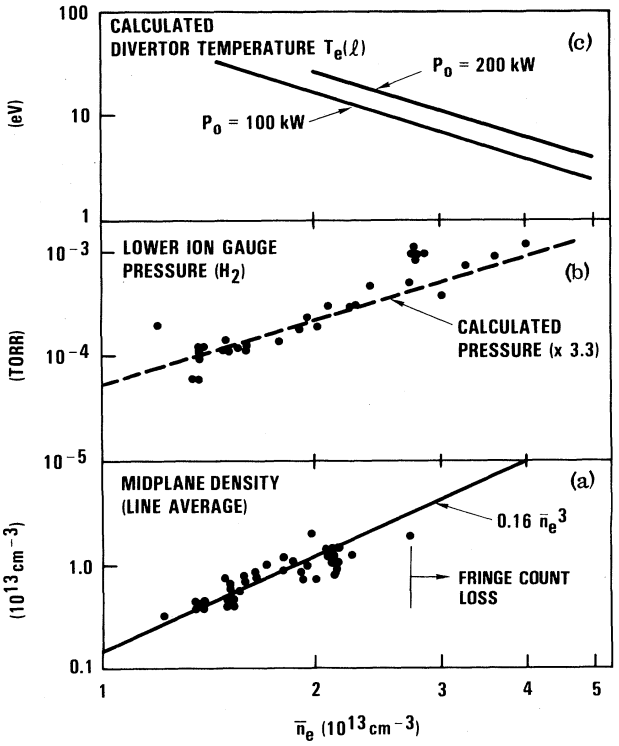

FIG. 2. Density dependence of divertor plasma parameters. (a) Midplane line-average density; the solid line shows the best fit of experimental data to the model. (b) Ion gauge pressure (lower chamber). (c) Calculated divertor temperatures for two estimates of power flowing to the plasma boundary.

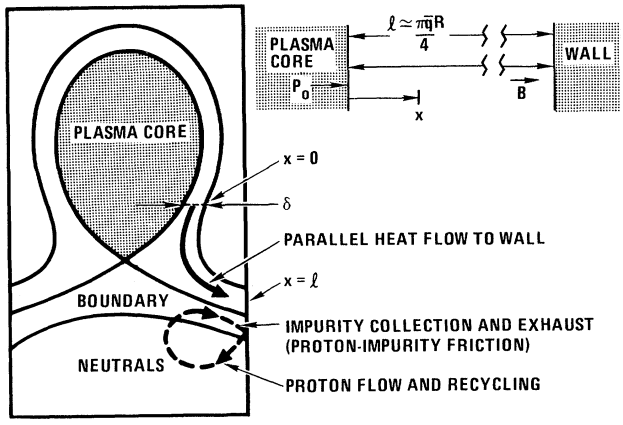

FIG. 3. Schematic representation of the boundary heat and particle flows.

the plasma parameters at the target are

$$T_e(l) = \frac{2\pi M_i}{(7l/2\kappa_0)^{4/7}k^3\gamma^2\alpha^2}\left(\frac{P_0}{A}\right)^{10/7}\bar{n}_e^{-2} \quad (3)$$

and

$$n_e(l) = \frac{\gamma^2 k^3\alpha^3}{2\pi M_i}\left(\frac{7l}{2\kappa_0}\right)^{6/7}\left(\frac{A}{P_0}\right)^{8/7}\bar{n}_e^{3}. \quad (4)$$

The temperature in the divertor region $T_e(l)$ scales as $\bar{n}_e^{-2}$, and the density in the divertor region scales as $\bar{n}_e^3$. This cubic scaling of $n_e(l)$ is consistent with the data of Fig. 2(a). Fitting the data of Fig. 2(a) by Eq. (4) yields $n_e(l) = 0.16\bar{n}_e^3$ where n_e is in units of 10^{13} cm^{-3}. With use of this result, $T_e(l)$ can be calculated directly from the boundary condition at $x = l$. We obtain $T_e(l) = 63P_0^{2/3}\bar{n}_e^{-2}$, where P_0 is in units of 10^5 W, and $T_e(l)$ in electron volts. Calculated values of $T_e(l)$ are shown in Fig. 2(c) for two values of P_0. For the upper curve, $P_0 = 200$ kW is the difference between the Ohmic input power and the total power radiated from within the closed flux surfaces of the discharge, as measured with a bolometer array. For the lower curve, $P_0 = 100$ kW is estimated from thermocouple measurements of the energy flux to the outer midplane wall.

The results of the model can be used to estimate the steady-state atomic hydrogen density, $n_0(\mathrm{H})$, in the lower chamber. Hydrogen flux balance between the plasma and the lower chamber yields

$$n_0(\mathrm{H}) \simeq \frac{B_p(0)}{2CB_T}n_e(l)\frac{4\pi R\delta}{A_m}\left[\frac{T_e(l)}{T(\mathrm{H})}\right]^{1/2} \propto \frac{\bar{n}_e^{\,2}}{[T(\mathrm{H})]^{1/2}}, \quad (5)$$

where A_m is the cross-sectional area of the vacuum chamber at the midplane, $T(\mathrm{H})$ is the neutral atomic hydrogen temperature in the lower chamber, and C is a factor of $\sim\frac{1}{2}$ to account for charge-exchange effects. The pressure P_G is measured with an ionization gauge located 1 m from the vacuum chamber, where the neutrals can be safely assumed to be at the vessel temperature. From Eq. (5), the requirement for particle flux balance between the gauge and lower chamber leads to $P_G \propto \bar{n}_e^2$. The magnitude and density dependence of P_G is in reasonable agreement with Eq. (5) [Fig. 2(b)].

The impurity exhaust function of the divertor was studied by injection of a trace level of argon into the discharge. A 1-msec burst ($\sim 10^{17}$ atoms) of argon was injected into both diverted discharges, hereafter referred to as XB "on," and nondiverted discharges (XB "off"). The argon concentration in the discharge was monitored by measuring the intensity of line radiation from Ar XV (221 Å) and Ar XVI (354 Å) normalized by $\bar{n}_e$. For XB "off" discharges the argon concentration rose to a steady-state level within ~ 50 msec after injection. A similar behavior was observed for Ar VII (586 Å) radiation. For XB "on," the Ar XV radiation increased to an initial peak, typically half of the XB "off" level, in about 30 msec and then decayed with a time constant of 50 msec to a lower, steady-state level. The decay of argon in the main discharge coincides with a rise of neutral argon in the lower chamber.[4] In each configuration the behavior of Ar VII (586 Å) radiation was similar to that of the higher ionization stages.

Argon exhaust ratio is defined as the ratio of the steady-state level of (Ar XV)/$\bar{n}_e$ for XB "off" to XB "on." As shown in Fig. 4, the exhaust ratio improves with increasing $\bar{n}_e$. For XB "on" at low densities, the argon concentration is comparable to the XB "off" case; however, as density exceeds 1.5×10^{13} cm^{-3}, the argon concentration begins to fall at high density; the exhaust ratio is ~ 10. The argon exhaust ratio is further enhanced by more intensive gas puffing, as shown

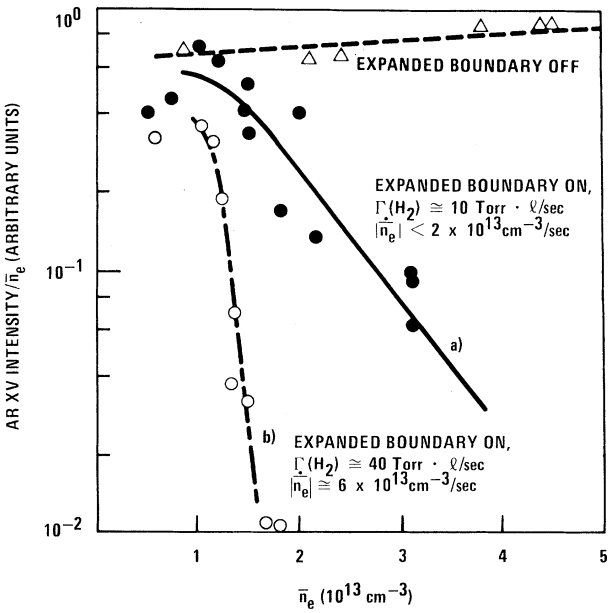

FIG. 4. Density dependence of argon concentration in diverted discharges (curve *a*) at H_2 injection rate of ~ 10 Torr • L/sec and (curve *b*) at ~ 40 Torr • L/sec. The top trace shows the density dependence of argon concentration in a nondiverted discharge with an H_2 injection rate of ~ 10 Torr • L/sec.

in Fig. 4. The argon exhaust results are not significantly altered when the position of H_2 gas puffing is switched from the top to the bottom of the chamber.

Since the injected argon is accounted for at the end of the discharge,[4] argon removed from the main plasma can accumulate either as ions in the divertor region or as neutrals in the lower chamber. With use of the same procedure as was used to obtain Eq. (5), and energy reflectivity[5] from the walls of ~100% for argon particles with energies $\lesssim 50$ eV, it can be shown that most of the argon removed from the main discharge accumulates in ionic form in the divertor region. The accumulation of argon in the divertor can be explained by the effect of proton-argon frictional force. Near the wall (within an ionization mean free path of hydrogen) there is a strong proton flow. An estimate of the strength of the argon drag due to this flow may be obtained from the equation $\nabla_{\parallel} P_{\mathrm{Ar}} \sim (M_{\mathrm{Ar}} n_{\mathrm{Ar}} / \tau_{\mathrm{Ar}\text{-}p}) u_p$ where $\tau_{\mathrm{Ar}\text{-}p}$ is the argon-proton collision time, and $u_p \simeq (T_p / 2\pi M_p)^{1/2}$. The neutral argon ionization mean free path is always much shorter than the hydrogen mean free path λ_{H}, and the argon ion density gradient length is $L \equiv (n_{\mathrm{Ar}}{}^{-1} \partial n_{\mathrm{Ar}} / \partial x_{\parallel})^{-1} \sim (2 \times 10^3 / \bar{n}_e{}^7)$ where L is in units of centimeters and $\bar{n}_e$ in 10^{13} cm^{-3}, and we have used the results of Eqs. (3) and (4). The drag force is effective when $L < \lambda_{\mathrm{H}}(B_T/B_p)$. This condition is satisfied for $\bar{n}_e \gtrsim 1.2 \times 10^{13}$ cm^{-3}, a value very similar to that for the onset of argon exhaust in Fig. 4.

The phenomena of plasma density and neutral buildup in the divertor region are qualitatively similar to density and neutral accumulation observed near the limiter of nondiverted discharges in Doublet III[6] and other tokamaks.[7] Similar observations were made in a single null poloidal divertor configuration.[3] In the normally limited discharges most of the impurity neutrals penetrate the uninterrupted flux surfaces, thus reducing the effectiveness of the parallel proton flow on the impurity exhaust. In contrast, in the expanded-boundary configuration most of the impurity neutrals are ionized in a thick plasma layer separating the target plate and closed flux surfaces so that the impurities do not reach the main plasma.

In summary, with the expanded-boundary simplified divertor, we have observed that plasma density and neutral pressure in the divertor region rise nonlinearly with the line-average density of the main plasma. The density dependence of the divertor parameters is well described by a one-dimensional parallel heat-flow model with finite electron conductivity that neglects convection except near the divertor target. We also have observed efficient exhaust of trace levels of argon injected into the discharge, and show that argon-proton frictional force, calculated using the results of the heat-flow model, can explain the density dependence of the argon exhaust.

The authors wish to acknowledge Dr. T. Ohkawa's significant contributions to the expanded boundary concept and his continuing encouragement throughout this work, and to thank Dr. T. Jensen, Dr. R. Freeman, and Dr. K. Burrell for valuable discussions. We gratefully acknowledge the capable assistance of the Doublet III group members.

This work was supported by the U. S. Department of Energy under Contract No. DE-AT03-76ET51011.

[1]N. Ohyabu, Nucl. Fusion 21, 5 (1981).

[2]M. Ali Mahdavi *et al.*, in Proceedings of the Eighth International Conference on Plasma Physics and Controlled Nuclear Fusion Research, Brussels, Belgium, July 1980 (to be published), International Atomic Energy Agency Report No. IAEA-CN-3810-2, Part II.

[3]M. Nagami *et al.*, in Proceedings of the Eighth International Conference on Plasma Physics and Controlled Nuclear Fusion Research, Brussels, Belgium, July 1980 (to be published), International Atomic Energy Agency Report No. IAEA-CN-3810-2, Part I.

[4]N. Ohyabu *et al.*, General Atomic Company Report No. GA-A16355, 1981 (unpublished).

[5]C. M. McCracken and P. E. Stott, Nucl. Fusion 19, 889 (1979).

[6]D. Baker *et al.*, General Atomic Company Report No. GA-A16337, June 1981 (unpublished).

[7]D. O. Overskei, Phys. Rev. Lett. 46, 177 (1981).